

Epitaxial integration of high-mobility La-doped BaSnO₃ thin films with silicon F


Cite as: APL Mater. **7**, 022520 (2019); <https://doi.org/10.1063/1.5054810>

Submitted: 03 September 2018 • Accepted: 16 October 2018 • Published Online: 22 January 2019

Zhe Wang, Hanjong Paik,  Zhen Chen, et al.

COLLECTIONS

Paper published as part of the special topic on [Wide Bandgap Oxides](#)

 This paper was selected as Featured



View Online



Export Citation



CrossMark

ARTICLES YOU MAY BE INTERESTED IN

[Adsorption-controlled growth of La-doped BaSnO₃ by molecular-beam epitaxy](#)

APL Materials **5**, 116107 (2017); <https://doi.org/10.1063/1.5001839>

[High-mobility BaSnO₃ grown by oxide molecular beam epitaxy](#)

APL Materials **4**, 016106 (2016); <https://doi.org/10.1063/1.4939657>

[Effects of vacuum annealing on the electron mobility of epitaxial La-doped BaSnO₃ films](#)

APL Materials **7**, 022507 (2019); <https://doi.org/10.1063/1.5054154>

APL Materials

SPECIAL TOPIC:
Materials Challenges for Supercapacitors

Submit Today!



Epitaxial integration of high-mobility La-doped BaSnO₃ thin films with silicon

Cite as: APL Mater. 7, 022520 (2019); doi: 10.1063/1.5054810

Submitted: 3 September 2018 • Accepted: 16 October 2018 •

Published Online: 22 January 2019



View Online



Export Citation



CrossMark

Zhe Wang,^{1,a)} Hanjong Paik,^{2,3,a)} Zhen Chen,¹  David A. Muller,^{1,4} and Darrell C. Schlom^{2,4,b)}

AFFILIATIONS

¹School of Applied and Engineering Physics, Cornell University, Ithaca, New York 14853, USA

²Department of Materials Science and Engineering, Cornell University, Ithaca, New York 14853, USA

³Platform for the Accelerated Realization, Analysis, and Discovery of Interface Materials (PARADIM), Cornell University, Ithaca, New York 14853, USA

⁴Kavli Institute at Cornell for Nanoscale Science, Ithaca, New York 14853, USA

^{a)}**Contributions:** Z. Wang and H. Paik contributed equally to this work.

^{b)}**Author to whom correspondence should be addressed:** schlom@cornell.edu

ABSTRACT

La-doped BaSnO₃ has been epitaxially integrated with (001) Si using an SrTiO₃ buffer layer via molecular-beam epitaxy (MBE). A 254 nm thick undoped BaSnO₃ buffer layer was grown to enhance the mobility of the overlying La-doped BaSnO₃ layer. The x-ray diffraction rocking curve of the BaSnO₃ 002 peak has a full width at half maximum of 0.02°. At room temperature, the resistivity of the La-doped BaSnO₃ film is $3.6 \times 10^{-4} \Omega \text{ cm}$ and the mobility is $128 \text{ cm}^2 \text{ V}^{-1} \text{ s}^{-1}$ at a carrier concentration of $1.4 \times 10^{20} \text{ cm}^{-3}$. These values compare favorably to those of La-doped BaSnO₃ films grown by all techniques other than MBE on single-crystal oxide substrates. Our work opens an exciting arena for integrating hyper-functional oxide electronics that make use of high-mobility oxide films with the workhorse of the semiconductor industry, silicon.

© 2019 Author(s). All article content, except where otherwise noted, is licensed under a Creative Commons Attribution (CC BY) license (<http://creativecommons.org/licenses/by/4.0/>). <https://doi.org/10.1063/1.5054810>

Recently there has been tremendous interest in La-doped BaSnO₃ because of its unusually high mobility at room temperature for a transparent conducting oxide. Mobilities in La-doped BaSnO₃ single crystals¹ and thin films² have reached $320 \text{ cm}^2 \text{ V}^{-1} \text{ s}^{-1}$ and $183 \text{ cm}^2 \text{ V}^{-1} \text{ s}^{-1}$, respectively. The high room-temperature mobility of La-doped BaSnO₃, in combination with its transparency at optical wavelength, ability to be heavily doped, and oxygen stability^{1,3-6} makes it an exciting component for fabricating novel thermally stable devices including power electronics,^{7,8} optoelectronic devices,⁹⁻¹¹ thermoelectric devices,¹² solar cells,¹³ and field effect transistors.^{14,15} Moreover, thanks to the structural and chemical compatibility of BaSnO₃ with functional perovskite oxides that show a plethora of novel and emergent properties, a heterostructure consisting of high-mobility La-doped BaSnO₃, and other perovskite oxides can potentially enrich the family of functionalities of all-oxide heterostructures and provide opportunities for hybrid devices by exploiting emergent

phenomena of oxide interfaces and heterostructures.^{16,17} For example, integration of high mobility La-doped BaSnO₃ with ferroelectrics such as Pb(Zr, Ti)O₃ can potentially realize devices including nonvolatile memories,¹⁸ ferroelectric field-effect transistors,¹⁹ low-power transistors that can beat the 60 mV/decade subthreshold slope limit of conventional semiconductors,²⁰ and hyper-sensitive temperature or pressure sensors.²¹

While rapid progress has been made on the growth of high-mobility BaSnO₃ thin films during the last few years,^{1,2,22-28} most of the La-doped BaSnO₃ thin films have been grown on single-crystal oxide substrates which are currently limited to small size (typically no larger than $10 \times 10 \text{ nm}$). Very limited work on La-doped BaSnO₃ thin films has been carried out on scalable substrates of industrial quality,²⁹ thus making it difficult to take advantage of the well-developed and efficient fabrication processes in the semiconductor industry.

Specifically, there is no report of growing La-doped BaSnO₃ films on the backbone of semiconductor industry, silicon.

The integration of functional oxides directly on silicon, however, is difficult due to the reactive nature of the (001) Si surface with oxygen to form an amorphous SiO₂ layer that can impede epitaxial growth. Furthermore, most oxides react with silicon. Due to the unknown free energy of BaSnO₃, we are unable to assess its thermodynamic stability in direct contact with silicon. We note, however, that the binary components of BaSnO₃-BaO and SnO₂-are both thermodynamically unstable in contact with silicon.³⁰ From a simple bond strength perspective, where energies are assigned to M-O bonds (where M is a cation), this would suggest that BaSnO₃ is unstable in direct contact with silicon.³¹ The lack of thermodynamic stability does not, however, preclude epitaxial growth. The epitaxial growth of an unstable interface can sometimes be achieved at low temperature, e.g., room temperature as is used to form epitaxial BaO/Si³² or CeO₂/Si interfaces,³³ both of which are thermodynamically unstable. Upon heating to about 650 °C, however, reaction is observed at these interfaces following the expectations of thermodynamics.^{30,34-37}

To date, only a few oxides have been epitaxially grown directly on silicon. These include BeO,^{38,39} MgO,^{40,41} SrO,^{36,42} BaO,^{32,43} Sc₂O₃,⁴⁴ Y₂O₃,⁴⁵ ZrO₂,⁴⁶ HfO₂,⁴⁷ La₂O₃,⁴⁸ CeO₂,³³ Pr₂O₃,^{49,50} Nd₂O₃,^{51,52} Sm₂O₃,⁵³ EuO,^{54,55} Gd₂O₃,⁵⁶⁻⁵⁸ Dy₂O₃,⁵³ Ho₂O₃,⁵³ Er₂O₃,^{58,59} Tm₂O₃,⁶⁰ Lu₂O₃,⁶¹ Al₂O₃,⁶² yttria-stabilized zirconia (YSZ),⁶³ yttria-stabilized hafnia (Y₂O₃-HfO₂),⁶⁴ (Ba, Sr)O,^{36,43} (La, Y)₂O₃,⁶⁵ (Pr, Y)₂O₃,⁶⁶ (La, Lu)₂O₃,⁶⁷⁻⁶⁹ MgAl₂O₄,⁷⁰ SrTiO₃,^{71,72} La₂Zr₂O₇,⁷³ SrHfO₃,^{74,75} Ba₂SiO₄,³⁷ and La₂Hf₂O₇.⁷⁶ Among these, SrTiO₃ is one of the most frequently used epitaxial buffer layers for the growth of functional oxides on (001) Si,⁷⁷ thanks to its relatively high crystalline quality on silicon⁷⁸⁻⁸⁰ and its structural compatibility with various functional perovskite materials.^{77,81}

Here we report growth of La-doped BaSnO₃ films on (001) Si using a SrTiO₃ buffer layer grown by molecular-beam epitaxy (MBE). The resulting La-doped BaSnO₃ film on silicon is epitaxial, with a room-temperature mobility of 128 cm² V⁻¹ s⁻¹ and a resistivity of 3.6 × 10⁻⁴ Ω cm, at a carrier concentration of 1.4 × 10²⁰ cm⁻³. Both the structural perfection and the electrical transport characteristics of the La-doped BaSnO₃ films on silicon rival those of epitaxial La-doped BaSnO₃ films grown on single-crystal oxide substrates.^{1,2,5-7,14,22-29,82-84}

The SrTiO₃ buffer layer and the La-doped BaSnO₃ film were grown in a Veeco GEN10 dual-chamber MBE system. Each growth chamber is equipped with an *in situ* reflection high-energy electron diffraction (RHEED) system for monitoring the film growth. Substrate temperature is monitored with a thermocouple for temperatures below 500 °C and an optical pyrometer with a measurement wavelength of 980 nm for temperatures above 500 °C. The silicon substrates (2" diameter, *p*-type, boron doped, and with resistivity larger than 10 Ω cm) were cleaned in an ultraviolet ozone cleaner for 20 min before being loaded into the first growth chamber with a background pressure in the upper 10⁻⁹ Torr range.

An 18 nm thick SrTiO₃ buffer layer was grown on the bare (001) Si. The first 2 nm were grown using the epitaxy-by-periodic-annealing method^{85,86} followed by an additional 16 nm grown by codeposition at 580 °C under an oxygen partial pressure of ~ (5 - 8) × 10⁻⁸ Torr. Elemental strontium and titanium beams were generated from a conventional low-temperature effusion cell and a Ti-Ball,⁸⁷ respectively. To be specific, two 2.5 unit-cell-thick SrTiO₃ layers were grown by codeposition (strontium, titanium, and oxygen all supplied simultaneously) at 300 °C under an oxygen partial pressure of ~ 5 × 10⁻⁸ Torr, then the substrate temperature was raised to 580 °C under vacuum to enhance the crystalline quality of the as-grown SrTiO₃ film. After forming a 5 unit-cell-thick epitaxial SrTiO₃ film (i.e., two repeats of the epitaxy-by-periodic-annealing step) by this process, the substrate temperature was raised to 580 °C and additional SrTiO₃ was codeposited until the SrTiO₃ film reached a total thickness of 18 nm. RHEED patterns of the 18 nm thick SrTiO₃ film viewed along the [100] and [110] azimuths are shown in Figs. 1(a) and 1(b), respectively. No other phases were detected during or after the growth of the 18 nm thick SrTiO₃ film, indicating that the SrTiO₃ film is a single phase and epitaxial. More detail of the growth of the SrTiO₃ buffer layer on silicon is provided elsewhere.⁸⁰

The (La-doped) BaSnO₃ films are grown in an adsorption-controlled regime, with molecular beams emanating from separate effusion cells containing lanthanum (99.996% purity, Ames Lab), barium (99.99% purity, Sigma-Aldrich), and SnO₂ (99.996% purity, Alfa Aesar).² The oxidant used for the growth of the (La-doped) BaSnO₃ films is a mixture of ~10% ozone and 90% oxygen. By growing BaSnO₃ within an adsorption-controlled regime, the stoichiometry of the BaSnO₃ film is ensured by exploiting the volatility of the SnO_x(g): excess

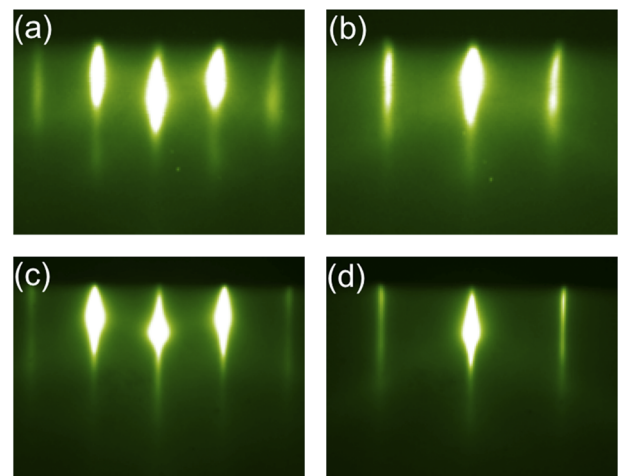


FIG. 1. RHEED patterns viewed along (a) the [100] azimuth and (b) the [110] azimuth of the 18 nm thick (001)-oriented SrTiO₃ buffer layer after growth. (c) RHEED patterns viewed along (c) the [100] azimuth and (d) the [110] azimuth of the overlying 318 nm thick BaSnO₃ film after growth.

$\text{SnO}_x(\text{g})$ leaves the surface of the growing film so that a stoichiometric BaSnO_3 film is formed.² During the growth of the (La-doped) BaSnO_3 , all components—(lanthanum), barium, SnO_x , and the $\sim 10\% \text{O}_3 + 90\% \text{O}_2$ oxidant—are supplied simultaneously, and the substrate temperature is kept at $\sim 700^\circ\text{C}$. RHEED intensity oscillations (Fig. S1) were observed during the initial codeposition growth stage of the BaSnO_3 film on the SrTiO_3 buffer layer on silicon, manifesting a layer-by-layer growth mode of the BaSnO_3 film on SrTiO_3 -buffered silicon at the initial growth stage.² A 254 nm thick undoped BaSnO_3 buffer layer is deposited on top of the 18 nm thick SrTiO_3 buffer layer, followed by a 64 nm thick active layer of La-doped BaSnO_3 . The purpose of the thick undoped BaSnO_3 layer is to enhance the electron mobility of the active layer.^{14,25,83} Further details on the growth of the (La-doped) BaSnO_3 films can be found elsewhere.²

RHEED patterns after the growth of the 64 nm thick La-doped BaSnO_3 on the 254 nm thick undoped BaSnO_3 buffer layer are shown in Figs. 1(c) and 1(d). The streaky RHEED patterns indicate that the surface of the La-doped BaSnO_3 film is epitaxial and relatively smooth on an atomic scale. The 1×1 surface reconstruction of the La-doped BaSnO_3 film observed in RHEED that is sharp and free of diffuse features manifest that the La-doped BaSnO_3 film is stoichiometric.² The surface morphology of the same sample was examined *ex situ* by atomic force microscopy (AFM) using an Asylum Research MFP-3D in tapping mode, as is shown in Fig. S2. The rms roughness of the sample is $\sim 4 \text{ \AA}$, which is consistent with the streaky RHEED patterns.

The crystalline quality of the same sample was assessed by *ex-situ* x-ray diffraction (XRD) with a PANalytical X'Pert system utilizing $\text{Cu K}\alpha_1$ radiation. Figure 2(a) shows the θ - 2θ scan of the same heterostructure characterized in Fig. 1. Only 00l reflections of the SrTiO_3 buffer layer and the BaSnO_3 film are

observed in the θ - 2θ scan, corroborating that the film is epitaxial and phase pure. A fine θ - 2θ scan around the BaSnO_3 002 peak is shown in Fig. 2(b). Clear thickness fringes around the BaSnO_3 002 peak manifest that the interfaces of the sample are smooth. Using a Nelson-Riley analysis,⁸⁸ the out-of-plane lattice parameter of the BaSnO_3 film is calculated to be $4.110 \pm 0.001 \text{ \AA}$, which is close to, but slightly smaller than the bulk value of 4.116 \AA .⁸⁹

We believe the slightly smaller out-of-plane lattice parameter of the BaSnO_3 film is due to the tensile strain caused by the relatively large difference between the thermal expansion coefficients of BaSnO_3 (averaging $9.3 \times 10^{-6} \text{ K}^{-1}$ between room temperature to 1500°C)⁹⁰ and silicon (averaging $3.7 \times 10^{-6} \text{ K}^{-1}$ between room temperature and 720°C).⁹¹ To verify this, we calculate the expected out-of-plane lattice parameter of the BaSnO_3 film at room temperature ($a_{\text{out-of-plane},25^\circ\text{C}}^{\text{BaSnO}_3}$) and the expected tensile strain under the assumptions that the BaSnO_3 film is fully relaxed at the growth temperature ($\sim 700^\circ\text{C}$) and that the BaSnO_3 film is rigidly clamped to the underlying silicon substrate as it is cooled to room temperature.

From

$$a_{\text{in-plane},25^\circ\text{C}}^{\text{BaSnO}_3} - a_{\text{in-plane},700^\circ\text{C}}^{\text{BaSnO}_3} = \frac{a_{\text{in-plane},25^\circ\text{C}}^{\text{silicon}} - a_{\text{in-plane},700^\circ\text{C}}^{\text{silicon}}}{\sqrt{2}}, \quad (1)$$

where $a_{\text{in-plane},25^\circ\text{C}}^{\text{silicon}} = 5.4305 \text{ \AA}$ is the silicon lattice parameter at room temperature, $a_{\text{in-plane},700^\circ\text{C}}^{\text{silicon}} = 5.444 \text{ \AA}$ is the silicon lattice parameter at the growth temperature, and $a_{\text{in-plane},700^\circ\text{C}}^{\text{BaSnO}_3} = 4.142 \text{ \AA}$ is the in-plane lattice parameter of the BaSnO_3 film at the growth temperature, we can calculate the expected

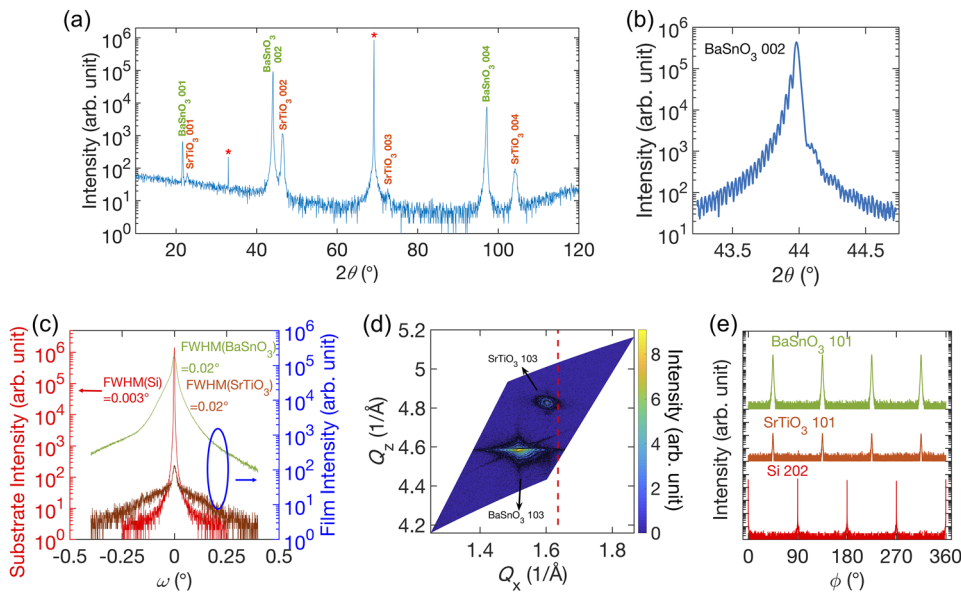


FIG. 2. (a) XRD θ - 2θ scan of the same sample characterized in Fig. 1. The asterisks indicate the substrate peaks. (b) An enlarged view of the θ - 2θ scan around the BaSnO_3 002 peak with clear thickness fringes. The θ - 2θ scan was measured with an open detector, and the fine scan around the BaSnO_3 002 peak was measured in a triple-axis geometry. (c) Rocking curves of the SrTiO_3 and BaSnO_3 002 peaks, together with that of the Si 004 peak. The FWHM of both the SrTiO_3 and the BaSnO_3 002 peaks is 0.02° . The FWHM of the Si 004 peak is 0.003° . (d) RSM around the BaSnO_3 and SrTiO_3 103 peaks. (e) ϕ scan of the same sample. The Si 202, SrTiO_3 101, and BaSnO_3 101 family of peaks were measured, and the FWHM of the film ϕ scans is 0.9° for both the SrTiO_3 101 and BaSnO_3 101 peaks. The ϕ scans are offset from each other along the vertical axis for clarity.

in-plane lattice parameter of the BaSnO₃ film, $a_{in-plane,25^\circ C}^{BaSnO_3} = 4.132 \text{ \AA}$.

Using

$$a_{out-of-plane,25^\circ C}^{BaSnO_3} = \frac{2\nu}{\nu-1} a_{in-plane,25^\circ C}^{BaSnO_3} + \frac{1+\nu}{1-\nu} a_{0,25^\circ C}^{BaSnO_3} \quad (2^{92,93})$$

where $a_{0,25^\circ C}^{BaSnO_3} = 4.116 \text{ \AA}$ is the bulk lattice parameter of BaSnO₃, ν is Poisson's ratio of BaSnO₃ (here we use a value $\nu = 0.23$ obtained from first-principles calculations),⁹⁴ we get $a_{out-of-plane,25^\circ C}^{BaSnO_3} = 4.106 \text{ \AA}$, which is close to the out-of-plane lattice parameter we obtained from the XRD measurement ($4.110 \pm 0.001 \text{ \AA}$). Note that the agreement would be improved if some relaxation occurred in the BaSnO₃ film as it is cooled from growth temperature to room temperature.

Using $a_{in-plane,25^\circ C}^{BaSnO_3} = 4.132 \text{ \AA}$, we can also calculate the expected tensile strain on the BaSnO₃ film due to the thermal expansion difference. The expected tensile strain is 0.39%. Starting from this expected tensile strain, the expected critical thickness before mechanical cracks form can be calculated⁹⁵ using

$$h_c = \frac{a_0(1-\nu)^2}{5\pi \cdot f^2}, \quad (3)$$

where a_0 is the lattice parameter and f is the expected tensile strain, 0.39%. h_c is calculated to be $\sim 1.0 \text{ \mu m}$, which is larger than the thickness of our BaSnO₃ film. This is consistent with our observation by AFM that our film is free of cracks.

XRD rocking curves (ω scans) of the SrTiO₃ and BaSnO₃ 002 peaks together with that of the Si 004 peak were measured in a triple-axis geometry, and the results are shown superimposed in Fig. 2(c). Despite the large $\sim 5.4\%$ compressive strain for (001) BaSnO₃ on (001) SrTiO₃, the crystalline quality of the BaSnO₃ film is similar to that of the SrTiO₃ buffer layer: they both have a full width at half maximum (FWHM) of 0.02° of their rocking curve, which shows a high degree of crystalline perfection for both the SrTiO₃ buffer layer and the BaSnO₃ film. This can be attributed to the optimized growth process of the SrTiO₃ buffer layer⁸⁰ and the adsorption-controlled growth of the BaSnO₃ film to maintain its stoichiometry.² Figure 2(d) shows reciprocal space maps (RSMs) of the BaSnO₃ and SrTiO₃ 103 peaks. The red line in Fig. 2(d) shows the film in-plane reciprocal space position that the SrTiO₃ and BaSnO₃ films would have if they were commensurately strained to the silicon substrate. Both the in-plane and out-of-plane lattice parameters of the SrTiO₃ buffer layer and the BaSnO₃ film are found to be fully relaxed to their bulk values.

If the strain introduced by defects is highly anisotropic, as is the case for our SrTiO₃ grown on silicon,⁸⁰ characterizing them in a single direction (the out-of-plane direction by the 002 rocking curve) is insufficient. The narrow rocking curve of the 002 SrTiO₃ peak is because of the insensitivity of this particular peak to threading dislocations with pure edge character.⁸⁰ This conclusion also holds for the 002 BaSnO₃

peak of these BaSnO₃/SrTiO₃/Si films. The threading dislocation density of our SrTiO₃/Si films is in excess of 10^{11} cm^{-2} (Ref. 80) and as shown below so is the threading dislocation density of the BaSnO₃ film grown on the SrTiO₃/Si. To further characterize the structural perfection of these films in a different direction (in-plane rather than out-of-plane) ϕ -scans were used. These ϕ -scans assess the in-plane mosaic spread of the SrTiO₃ and BaSnO₃ layers as well as establish their epitaxial orientation relationship. The in-plane epitaxial orientation relationship of the heterostructure was confirmed to be cube-on-cube with a 45° in-plane rotation: (001) BaSnO₃ \parallel (001) SrTiO₃ \parallel (001) Si and [100] BaSnO₃ \parallel [100] SrTiO₃ \parallel [110] Si, as is shown in Fig. 2(e). The FWHM of the film ϕ scan is 0.9° for both the SrTiO₃ 101 peak and the BaSnO₃ 101 peak. Thus, reducing the in-plane mosaic spread remains the biggest challenge to overcome for both the BaSnO₃ and SrTiO₃ layers in this heterostructure.

The microstructure of the same sample including the abruptness of the interfaces was examined by scanning transmission electron microscopy (STEM), using a probe aberration corrected Titan electron microscope operating at 300 keV. Figure 3(a) is a high-angle annular dark field (HAADF) STEM image that shows the film microstructure in cross section. Threading dislocations in the BaSnO₃ film are illustrated from the stripe contrast in the low-angle annular dark field (LAADF) STEM image shown in Fig. S3. The density of the threading dislocation is estimated to be $\sim 1.3 \times 10^{11} \text{ cm}^{-2}$, which is similar to the La-doped BaSnO₃ films grown on single-crystal oxide substrates with large lattice mismatch.² The threading dislocations come from both the large lattice mismatch between (001) BaSnO₃ and (001) SrTiO₃, as well as the threading dislocations from the 18 nm thick SrTiO₃ buffer layer on silicon.

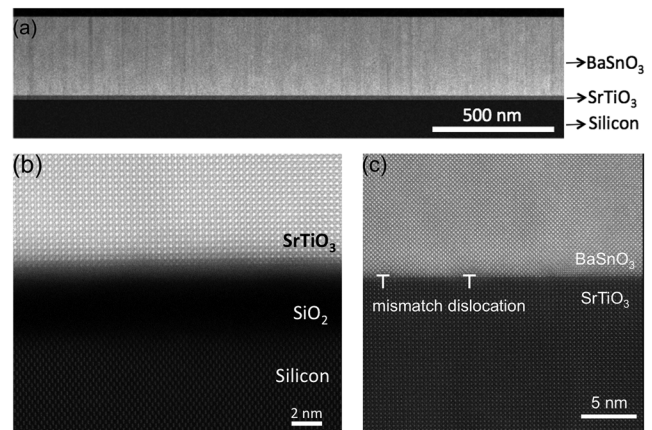


FIG. 3. STEM images showing the microstructure of the same sample characterized in Fig. 1. (a) HAADF-STEM image with a low magnification showing the overall sample. (b) The interface between the SrTiO₃ buffer layer and the silicon substrate shows that there is an amorphous SiO₂ layer between the SrTiO₃ buffer layer and the silicon substrate. (c) The interface between the BaSnO₃ film and the SrTiO₃ buffer layer is atomically sharp. Due to the large lattice mismatch between (001) BaSnO₃ and (001) SrTiO₃, there are misfit dislocations observed in the interface, two examples are marked by the edge dislocation symbols in (c).

The microstructure of the SrTiO₃/Si and the BaSnO₃/SrTiO₃ interfaces is shown in Figs. 3(b) and 3(c), respectively. There is a ~4 nm thick amorphous SiO₂ layer between the SrTiO₃ buffer layer and the silicon substrate, which originates from oxygen diffusion through the SrTiO₃ buffer layer during film growth. The extent of interdiffusion across the SrTiO₃/Si and BaSnO₃/SrTiO₃ interfaces was investigated by electron energy loss spectroscopy (EELS). As is shown in Fig. S4, there is no observable titanium interdiffusion into the SiO₂ layer. Line profiles of the elemental intensity of silicon, oxygen, and titanium across the SrTiO₃/Si interface are shown in Fig. S4(f). The HAADF image in Fig. 3(c) shows that the BaSnO₃/SrTiO₃ interface is abrupt and contains mismatch dislocations. The interface between the BaSnO₃ film and the SrTiO₃ buffer layer is fully relaxed, with an average spacing between edge dislocations of 22 unit cells of SrTiO₃ vs. 21 unit cells of BaSnO₃, which is consistent with the calculated ratio based on relaxed lattice parameters (~5.4%). EELS mappings of titanium and barium across the BaSnO₃/SrTiO₃ interface are shown in Fig. S5, and the corresponding line profiles shown in Fig. S5(e) also indicate a clean interface that is free of perceptible interdiffusion.

The transport properties of the same sample was measured in the van der Pauw geometry in a quantum design physical property measurement system (PPMS). Aluminum wires were wire-bonded directly to the La-doped BaSnO₃ film. Figure 4(a) shows the temperature-dependent resistivity. At room temperature, the resistivity is $3.6 \times 10^{-4} \Omega \text{ cm}$ (corresponding to a conductivity of $2.8 \times 10^3 \text{ S cm}^{-1}$). From 300 K to 10 K, the sample shows weak metallic behavior with no upturn of the resistivity at low temperature. The room temperature mobility of the sample is $128 \text{ cm}^2 \text{ V}^{-1} \text{ s}^{-1}$, which is comparable to most La-doped BaSnO₃ films grown on single-crystal oxide substrates.^{1,2,5-7,14,22-29,82-84} A comparison of the room temperature mobility of our La-doped BaSnO₃ film on silicon with those of representative La-doped BaSnO₃ films grown on single-crystal oxide substrates is shown in Fig. 4(d). We attribute the high mobility of the La-doped BaSnO₃ film on silicon to its high degree of crystalline perfection.¹¹ As the temperature decreases, the mobility increases, as is shown in Fig. 4(b). At room temperature, the carrier concentration is $1.4 \times 10^{20} \text{ cm}^{-3}$. From an extrapolated measurement of the lanthanum flux, made using a quartz crystal microbalance, and assuming that all of the incident lanthanum is incorporated into the La-doped BaSnO₃ film, the lanthanum concentration in the film is $(1.6 \pm 0.6)\%$. Comparing the lanthanum concentration to the measured concentration of mobile carriers ($1.4 \times 10^{20} \text{ cm}^{-3}$ electrons), the dopant activation percentage is $(64 \pm 25)\%$. Figure 4(c) shows that the carrier concentration of the La-doped BaSnO₃ film is almost temperature independent. The temperature-dependent resistivity, mobility, and carrier concentration of our film on silicon closely resemble those of La-doped BaSnO₃ films grown on single-crystal oxide substrates.^{1,2,5-7,14,22-29,82-84}

In summary, we have integrated La-doped BaSnO₃ films on silicon using an epitaxial SrTiO₃ buffer layer formed by MBE. The surface morphology, structural perfection, and

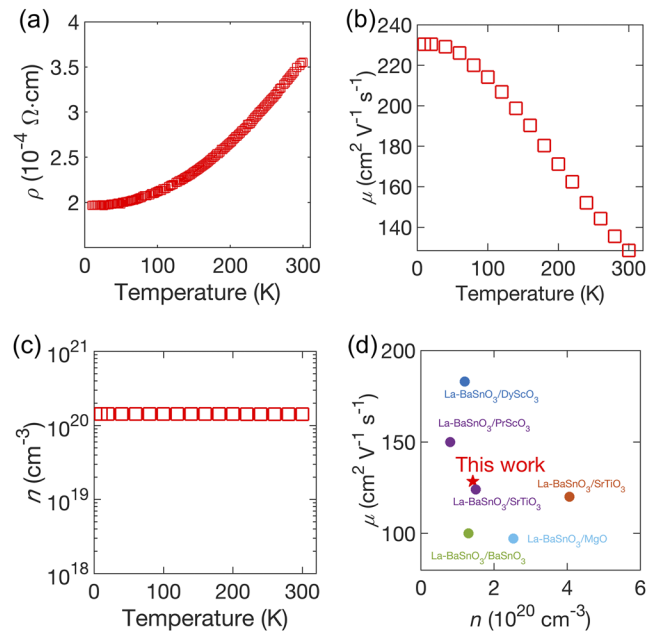


FIG. 4. Temperature-dependent (a) resistivity (ρ), (b) mobility (μ), and (c) carrier concentration (n) of the same sample characterized in Fig. 1. The results resemble those of La-doped BaSnO₃ films grown on single-crystal oxide substrates. (d) Comparison of the room-temperature mobility of our La-doped BaSnO₃ film on silicon (red star) with those of representative epitaxial BaSnO₃ films grown on single-crystal oxide substrates in the literature. μ is the mobility, and n is the carrier concentration of the La-doped BaSnO₃ films. The La-BaSnO₃/DyScO₃ data point is from Ref. 2; the La-BaSnO₃/PrScO₃ and the purple La-BaSnO₃/SrTiO₃ data points are from Ref. 24; the brown La-BaSnO₃/SrTiO₃ data point is from Ref. 7; the La-BaSnO₃/BaSnO₃ data point is from Ref. 26; the La-BaSnO₃/MgO data point is from Ref. 84.

electrical properties of our samples are similar to those of La-doped BaSnO₃ films grown on single-crystal oxide substrates. Our results motivate the integration of functional oxide devices utilizing the exceptional properties of BaSnO₃-based heterostructures (e.g., the possibility of ferroelectric field effect transistors) with the backbone of today's semiconductor industry, silicon.

See [supplementary material](#) for RHEED oscillations of BaSnO₃ on SrTiO₃ on silicon, surface morphology of the sample, and additional STEM images and EELS mappings of the sample.

This material is based on the work supported by the Air Force Office of Scientific Research under Award No. FA9550-16-1-0192. We also gratefully acknowledge the support from a GRO "functional oxides" project from the Samsung Advanced Institute of Technology. H.P., Z.C., and D.A.M. acknowledge support by the National Science Foundation [Platform for the Accelerated Realization, Analysis, and Discovery of Interface Materials (PARADIM)] under Cooperative Agreement No. DMR-1539918. This work made use of the Cornell Center for Materials Research (CCMR) Shared Facilities, which are

supported through the NSF MRSEC Program (No. DMR-1719875). Substrate preparation was performed in part at the Cornell NanoScale Facility, a member of the National Nanotechnology Coordinated Infrastructure (NNCI), which is supported by the NSF (Grant No. ECCS-1542081).

REFERENCES

- H. J. Kim, U. Kim, H. M. Kim, T. H. Kim, H. S. Mun, B.-G. Jeon, K. T. Hong, W.-J. Lee, C. Ju, and K. H. Kim, *Appl. Phys. Express* **5**, 061102 (2012).
- H. Paik, Z. Chen, E. Lochocki, A. Seidner H., A. Verma, N. Tanen, J. Park, M. Uchida, S. Shang, B.-C. Zhou, M. Brützam, R. Uecker, Z.-K. Liu, D. Jena, K. M. Shen, D. A. Muller, and D. G. Schlom, *APL Mater.* **5**, 116107 (2017).
- B. Ostrick, M. Fleischer, and H. Meixner, *J. Am. Ceram. Soc.* **80**, 2153 (1997).
- X. Luo, Y. S. Oh, A. Sirenko, P. Gao, T. A. Tyson, K. Char, and S.-W. Cheong, *Appl. Phys. Lett.* **100**, 172112 (2012).
- S. Ismail-Beigi, F. J. Walker, S.-W. Cheong, K. M. Rabe, and C. H. Ahn, *APL Mater.* **3**, 062510 (2015).
- W.-J. Lee, H. J. Kim, E. Sohn, H. M. Kim, T. H. Kim, K. Char, J. H. Kim, and K. H. Kim, *Phys. Status Solidi A* **212**, 1487 (2015).
- A. Prakash, P. Xu, A. Faghaninia, S. Shukla, J. W. Ager III, C. S. Lo, and B. Jalan, *Nat. Commun.* **8**, 15167 (2017).
- S. Salahuddin, K. Ni, and S. Datta, *Nat. Electron.* **1**, 442 (2018).
- D. S. Ginley and C. Bright, *MRS Bull.* **25**, 15 (2000).
- H. Hosono, *Thin Solid Films* **515**, 6000 (2007).
- W.-J. Lee, H. J. Kim, J. Kang, D. H. Jang, T. H. Kim, J. H. Lee, and K. H. Kim, *Annu. Rev. Mater. Res.* **47**, 391 (2017).
- J. Li, Z. Ma, R. Sa, and K. Wu, *RSC Adv.* **7**, 32703 (2017).
- S. S. Shin, E. J. Yeom, W. S. Yang, S. Hur, M. G. Kim, J. Im, J. Seo, J. H. Noh, and S. I. Seok, *Science* **356**, 167 (2017).
- U. Kim, C. Park, T. Ha, Y. M. Kim, N. Kim, C. Ju, J. Park, J. Yu, J. H. Kim, and K. Char, *APL Mater.* **3**, 036101 (2015).
- J. Yue, A. Prakash, M. C. Robbins, S. J. Koester, and B. Jalan, *ACS Appl. Mater. Interfaces* **10**, 21061 (2018).
- K. Krishnaswamy, L. Bjaalie, B. Himmetoglu, A. Janotti, L. Gordon, and C. G. Van de Walle, *Appl. Phys. Lett.* **108**, 083501 (2016).
- A. I. Khan, K. Chatterjee, B. Wang, S. Drapcho, L. You, C. Serrao, S. R. Bakaul, R. Ramesh, and S. Salahuddin, *Nat. Mater.* **14**, 182 (2015).
- M. Suzuki, *J. Ceram. Soc. Jpn.* **103**, 1099 (1995).
- J. L. Moll and Y. Tarui, *IEEE Trans. Electron Devices* **10**, 338 (1963).
- S. Salahuddin and S. Datta, *Nano Lett.* **8**, 405 (2008).
- Y.-R. Wu and J. Singh, *IEEE Trans. Electron Devices* **52**, 284 (2005).
- H. F. Wang, Q. Z. Liu, F. Chen, G. Y. Gao, W. Wu, and X. H. Chen, *J. Appl. Phys.* **101**, 106105 (2007).
- P. V. Wadekar, J. Alaria, M. O'Sullivan, N. L. O. Flack, T. D. Manning, L. J. Phillips, K. Durose, O. Lozano, S. Lucas, J. B. Claridge, and M. J. Rosseinsky, *Appl. Phys. Lett.* **105**, 052104 (2014).
- S. Raghavan, T. Schumann, H. Kim, J. Y. Zhang, T. A. Cain, and S. Stemmer, *APL Mater.* **4**, 016106 (2016).
- J. Shiozaki, K. Nishihara, K. Sato, and A. Tsukazaki, *AIP Adv.* **6**, 065305 (2016).
- W.-J. Lee, H. J. Kim, E. Sohn, T. H. Kim, J.-Y. Park, W. Park, H. Jeong, T. Lee, J. H. Kim, K.-Y. Choi, and K. H. Kim, *Appl. Phys. Lett.* **108**, 082105 (2016).
- A. Prakash, P. Xu, X. Wu, G. Haugstad, X. Wang, and B. Jalan, *J. Mater. Chem. C* **5**, 5730 (2017).
- A. V. Sanchela, M. Wei, H. Zensyo, B. Feng, J. Lee, G. Kim, H. Jeon, Y. Ikuhara, and H. Ohta, *Appl. Phys. Lett.* **112**, 232102 (2018).
- C. Shan, T. Huang, J. Zhang, M. Han, Y. Li, Z. Hu, and J. Chu, *J. Phys. Chem. C* **118**, 6994 (2014).
- K. J. Hubbard and D. G. Schlom, *J. Mater. Res.* **11**, 2757 (1996).
- D. G. Schom, C. A. Billman, J. H. Haeni, J. Lettieri, P. H. Tan, R. R. M. Held, S. Völk, and K. J. Hubbard, *Thin Films and Heterostructures for Oxide Electronics*, edited by S. B. Ogale (Springer, New York, 2005), pp. 31–78.
- R. A. McKee, F. J. Walker, J. R. Conner, E. D. Specht, and D. E. Zelmon, *Appl. Phys. Lett.* **59**, 782 (1991).
- M. Yoshimoto, K. Shimozono, T. Maeda, T. Ohnishi, M. Kumagai, T. Chikyow, O. Ishiyama, M. Shinohara, and H. Koinuma, *Jpn. J. Appl. Phys., Part 2* **34**, L688 (1995).
- T. Chikyow, S. M. Bedair, L. Tye, and N. A. El-Masry, *Appl. Phys. Lett.* **65**, 1030 (1994).
- D. P. Norton, C. Park, Y. E. Lee, and J. D. Budai, *J. Vac. Sci. Technol., B: Microelectron. Nanometer Struct.* **20**, 257 (2002).
- J. Lettieri, J. H. Haeni, and D. G. Schlom, *J. Vac. Sci. Technol., A* **20**, 1332 (2002).
- S. Islam, K. R. Hofmann, A. Feldhoff, and H. Pfnür, *Phys. Rev. Appl.* **5**, 054006 (2016).
- J. H. Yum, T. Akyol, M. Lei, D. A. Ferrer, T. W. Hudnall, M. Downer, C. W. Bielawski, G. Bersuker, J. C. Lee, and S. K. Banerjee, *J. Cryst. Growth* **334**, 126 (2011).
- S. M. Lee, J. H. Yum, E. S. Larsen, W. C. Lee, S. K. Kim, C. W. Bielawski, and J. Oh, *Sci. Rep.* **7**, 13205 (2017).
- D. K. Fork, F. A. Ponce, J. C. Tramontana, and T. H. Geballe, *Appl. Phys. Lett.* **58**, 2294 (1991).
- F. Niu, A. L. Meier, and B. W. Wessels, *J. Vac. Sci. Technol., B: Microelectron. Nanometer Struct.* **24**, 2586 (2006).
- Y. Kado and Y. Arita, *J. Appl. Phys.* **61**, 2398 (1987).
- Y. Kado and Y. Arita, in *Extended Abstracts of the 20th (1988 International) Conference on Solid State Devices and Materials* (Publication Office, Business Center for Academic Society Japan, Tokyo, 1988), p. 181.
- D. O. Klenov, L. F. Edge, D. G. Schlom, and S. Stemmer, *Appl. Phys. Lett.* **86**, 051901 (2005).
- H. Fukumoto, T. Imura, and Y. Osaka, *Appl. Phys. Lett.* **55**, 360 (1989).
- M. Morita, H. Fukumoto, T. Imura, Y. Osaka, and M. Ichihara, *J. Appl. Phys.* **58**, 2407 (1985).
- S. Migita, Y. Morita, W. Mizubayashi, and H. Ota, in *IEEE International Electron Devices Meeting (IEDM) (IEEE, 2010)*, pp. 11–15.
- L. F. Edge, W. Tian, V. Vaithyanathan, T. Heeg, D. G. Schlom, D. O. Klenov, S. Stemmer, J. G. Wang, and M. J. Kim, *ECS Trans.* **16**, 213 (2008).
- E. J. Tarsa, J. S. Speck, and McD. Robison, *Appl. Phys. Lett.* **63**, 539 (1993).
- J. P. Liu, P. Zaumseil, E. Bugiel, and H. J. Osten, *Appl. Phys. Lett.* **79**, 671 (2001).
- H. Nagata, M. Yoshimoto, T. Tsukahara, S. Gonda, and H. Koinuma, *Evolution of Thin-film and Surface Microstructure*, edited by C. V. Thompson, J. Y. Tsao, and D. J. Srolovitz (Materials Research Society Symposium Proceedings, 202, Pittsburgh, PA, 1991), p. 445.
- A. Fissel, Z. Elassar, O. Kirfel, E. Bugiel, M. Czernohorsky, and H. J. Osten, *J. Appl. Phys.* **99**, 074105 (2006).
- H. S. Craft, R. Collazo, Z. Sitar, and J. P. Maria, *J. Vac. Sci. Technol., B: Microelectron. Nanometer Struct.* **24**, 2105 (2006).
- J. Lettieri, V. Vaithyanathan, S. K. Eah, J. Stephens, V. Sih, D. D. Awschalom, J. Levy, and D. G. Schlom, *Appl. Phys. Lett.* **83**, 975 (2003).
- A. Schmehl, V. Vaithyanathan, A. Herrnberger, S. Thiel, C. Richter, M. Liberati, T. Heeg, M. Röckerath, L. F. Kourkoutis, S. Mühlbauer, P. Böni, D. A. Muller, Y. Barash, J. Schubert, Y. Idzerda, J. Mannhart, and D. G. Schlom, *Nat. Mater.* **6**, 882 (2007).
- J. Kwo, M. Hong, A. R. Kortan, K. T. Queeney, Y. J. Chabal, J. P. Mannaerts, T. Boone, J. J. Krajewski, A. M. Sergent, and J. M. Rosamilia, *Appl. Phys. Lett.* **77**, 130 (2000).
- H. J. Osten, A. Laha, M. Czernohorsky, E. Bugiel, R. Dargis, and A. Fissel, *Phys. Status Solidi A* **205**, 695 (2008).
- R. Dargis, D. Williams, R. Smith, E. Arkun, R. Roucka, A. Clark, and M. Leppy, *ECS J. Solid State Sci. Technol.* **1**, N24 (2012).
- R. Xu, Y. Y. Zhu, S. Chen, F. Xue, Y. L. Fan, X. J. Yang, and Z. M. Jiang, *J. Cryst. Growth* **277**, 496 (2005).

- ⁶⁰T. Ji, J. Cui, Z. B. Fang, T. X. Nie, Y. L. Fan, X. L. Li, Q. He, and Z. M. Jiang, *J. Cryst. Growth* **321**, 171 (2011).
- ⁶¹W. Guo, A. Allenic, Y. B. Chen, X. Q. Pan, W. Tian, C. Adamo, and D. G. Schlom, *Appl. Phys. Lett.* **92**, 072101 (2008).
- ⁶²M. Ishida, I. Katakabe, T. Nakamura, and N. Ohtake, *Appl. Phys. Lett.* **52**, 1326 (1988).
- ⁶³H. Fukumoto, T. Imura, and Y. Osaka, *Jpn. J. Appl. Phys., Part 2* **27**, L1404 (1988).
- ⁶⁴J. Y. Dai, P. F. Lee, K. H. Wong, H. L. W. Chan, and C. L. Choy, *J. Appl. Phys., Part 1* **94**, 912 (2003).
- ⁶⁵S. Guha, N. A. Bojarczuk, and V. Narayanan, *Appl. Phys. Lett.* **80**, 766 (2002).
- ⁶⁶G. Niu, P. Zaumseil, M. A. Schubert, M. H. Zoellner, J. Dabrowski, and T. Schroeder, *Appl. Phys. Lett.* **102**, 011906 (2013).
- ⁶⁷V. V. Afanas'ev, S. Shamuilia, M. Badylevich, A. Stesmans, L. F. Edge, W. Tian, D. G. Schlom, J. M. J. Lopes, M. Roeckerath, and J. Schubert, *Microelectron. Eng.* **84**, 2278 (2007).
- ⁶⁸V. V. Afanas'ev, M. Badylevich, A. Stesmans, A. Laha, H. J. Osten, A. Fissel, W. Tian, L. F. Edge, and D. G. Schlom, *Appl. Phys. Lett.* **93**, 192105 (2008).
- ⁶⁹T. Watahiki, F. Grosse, W. Braun, V. M. Kaganer, A. Proessdorf, A. Trampert, and H. Riechert, *Appl. Phys. Lett.* **97**, 031911 (2010).
- ⁷⁰M. Ihara, Y. Arimoto, M. Jifuku, T. Kimura, S. Kodama, H. Yamawaki, and T. Yamaoka, *J. Electrochem. Soc.* **129**, 2569 (1982).
- ⁷¹H. Mori and H. Ishiwara, *Jpn. J. Appl. Phys., Part 2* **30**, L1415 (1991).
- ⁷²R. A. McKee, F. J. Walker, and M. F. Chisholm, *Phys. Rev. Lett.* **81**, 3014 (1998).
- ⁷³J. W. Seo, J. Fompeyrine, A. Guiller, G. Norga, C. Marchiori, H. Siegwart, and J.-P. Locquet, *Appl. Phys. Lett.* **83**, 5211 (2003).
- ⁷⁴C. Rossel, B. Mereu, C. Marchiori, D. Caimi, M. Sousa, A. Guiller, H. Siegwart, R. Germann, J.-P. Locquet, J. Fompeyrine, D. J. Webb, Ch. Dieker, and J. W. Seo, *Appl. Phys. Lett.* **89**, 053506 (2006).
- ⁷⁵M. Sousa, C. Rossel, C. Marchiori, H. Siegwart, D. Caimi, J.-P. Locquet, D. J. Webb, R. Germann, J. Fompeyrine, K. Babich, J. W. Seo, and Ch. Dieker, *J. Appl. Phys.* **102**, 104103 (2007).
- ⁷⁶A. Dimoulas, G. Vellianitis, G. Mavrou, G. Apostolopoulos, A. Travlos, C. Wiemer, M. Fanciulli, and Z. M. Rittersma, *Appl. Phys. Lett.* **85**, 3205 (2004).
- ⁷⁷S.-H. Baek and C.-B. Eom, *Acta Mater.* **61**, 2734 (2013).
- ⁷⁸L. Zhang and R. Engel-Herbert, *Phys. Status Solidi RRL* **8**, 917 (2014).
- ⁷⁹L. Zhang, Y. Wang, and R. Engel-Herbert, *J. Appl. Phys.* **119**, 045301 (2016).
- ⁸⁰Z. Wang, D. Baek, B. Goodge, M. Zachman, X. Huang, X. Bai, C. M. Brooks, H. Paik, A. B. Mei, J. D. Brock, J. P. Maria, L. F. Kourkoutis, and D. G. Schlom, "Highly anisotropic distortion of epitaxial SrTiO₃ films on silicon due to defects," (unpublished).
- ⁸¹Y.-Y. Pai, A. Tylan-Tyler, P. Irvin, and J. Levy, *Rep. Prog. Phys.* **81**, 036503 (2018).
- ⁸²H. J. Kim, U. Kim, T. H. Kim, J. Kim, H. M. Kim, B.-G. Jeon, W.-J. Lee, H. S. Mun, K. T. Hong, J. Yu, K. Char, and K. H. Kim, *Phys. Rev. B* **86**, 165205 (2012).
- ⁸³C. Park, U. Kim, C. J. Ju, J. S. Park, Y. M. Kim, and K. Char, *Appl. Phys. Lett.* **105**, 203503 (2014).
- ⁸⁴J. Shin, Y. M. Kim, Y. Kim, C. Park, and K. Char, *Appl. Phys. Lett.* **109**, 262102 (2016).
- ⁸⁵H. Li, X. Hu, Y. Wei, Z. Yu, X. Zhang, R. Droopad, A. A. Demkov, J. Edwards, K. Moore, W. Ooms, J. Kulik, and P. Fejes, *J. Appl. Phys.* **93**, 4521 (2003).
- ⁸⁶M. P. Warusawithana, C. Cen, C. R. Sleasman, J. C. Woicik, Y. Li, L. F. Kourkoutis, J. A. Klug, H. Li, P. Ryan, L. P. Wang, M. Bedzyk, D. A. Muller, L. Q. Chen, J. Levy, and D. G. Schlom, *Science* **324**, 367 (2009).
- ⁸⁷C. D. Theis and D. G. Schlom, *J. Vac. Sci. Technol., A* **14**, 2677 (1996).
- ⁸⁸J. B. Nelson and D. P. Riley, *Proc. Phys. Soc.* **57**, 160 (1945).
- ⁸⁹F. G. Kinyanjui, S. T. Norberg, C. S. Knee, I. Ahmed, S. Hull, L. Buannic, I. Hung, Z. Gan, F. Blanc, C. P. Grey, and S. G. Eriksson, *J. Mater. Chem. A* **4**, 5088 (2016).
- ⁹⁰T. Maekawa, K. Kurosaki, and S. Yamanaka, *J. Alloys Compd.* **416**, 214 (2006).
- ⁹¹Y. S. Touloukian, R. Kirby, E. Taylor, and T. Lee, *Thermophysical Properties of Matter—the TPRC Data Series*, Vol. 13, Thermal Expansion-Nonmetallic Solids (IFI/Plenum, New York, 1977).
- ⁹²L. D. Landau and E. Lifshitz, *Theory of Elasticity*, 2nd ed., Course of Theoretical Physics Vol. 7 (Pergamon Press, 1986), p. 45.
- ⁹³L. B. Freund and S. Suresh, *Thin Film Materials: Stress, Defect Formation and Surface Evolution* (Cambridge University Press, 2004), p. 432.
- ⁹⁴A. Bouhemadou and K. Haddadi, *Solid State Sci.* **12**, 630 (2010).
- ⁹⁵J. W. Matthews and E. Klokholm, *Mater. Res. Bull.* **7**, 213 (1972).

Epitaxial integration of high-mobility La-BaSnO₃ thin films with silicon

Zhe Wang*,¹ Hanjong Paik*,^{2,3} Zhen Chen,¹ David A. Muller,^{1,4} and Darrell G. Schlom^{2,4,a)}

¹*School of Applied and Engineering Physics, Cornell University, Ithaca, New York, 14853, USA*

²*Department of Materials Science and Engineering, Cornell University, Ithaca, New York, 14853, USA*

³*Platform for the Accelerated Realization, Analysis, & Discovery of Interface Materials (PARADIM), Cornell University, Ithaca, New York 14853, USA*

⁴*Kavli Institute at Cornell for Nanoscale Science, Ithaca, New York, 14853, USA*

^{a)} **Author to whom correspondence should be addressed. Electronic mail: schlom@cornell.edu**

*** These authors contributed equally to this work**

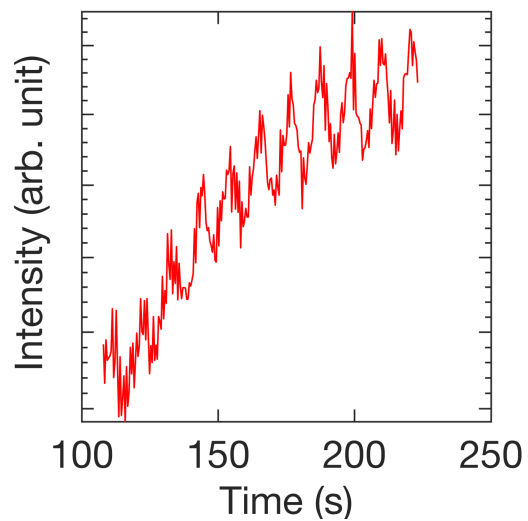


Fig. S1 RHEED oscillations of the BaSnO₃ film grown by codeposition during the initial growth stage on top of the 18 nm thick SrTiO₃ buffer layer on silicon. The oscillations indicate that the growth rate is ~ 0.374 Å/s.

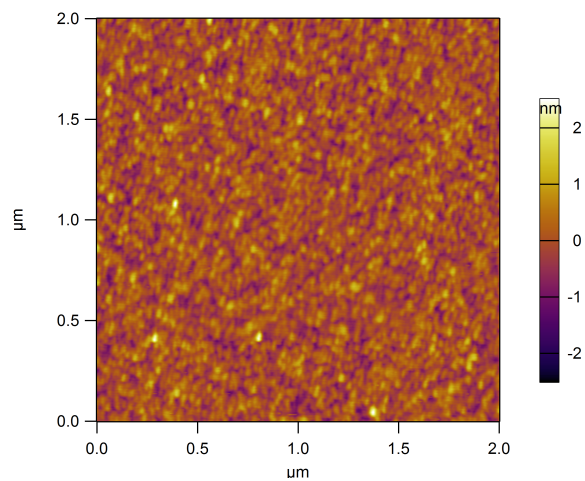


Fig. S2 Surface morphology revealed by AFM of the same sample characterized in Fig. 1. The rms roughness is ~ 4 Å.

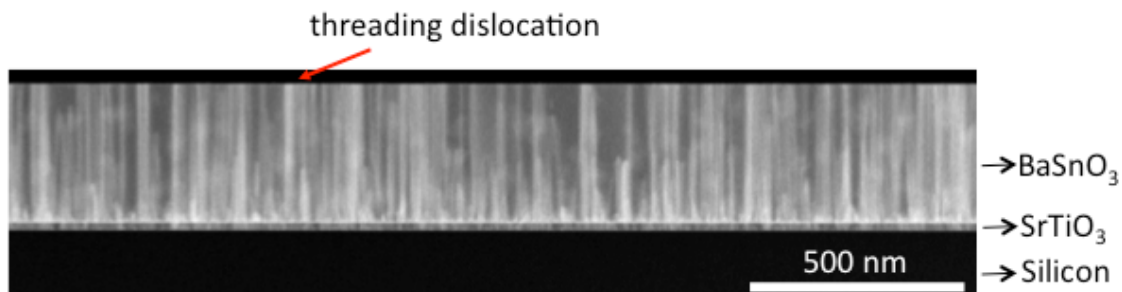


Fig. S3 LAADF-STEM image of the same sample characterized in Fig. 1 showing threading dislocations. The estimated dislocation density is $\sim 1.3 \times 10^{11} \text{ cm}^{-2}$.

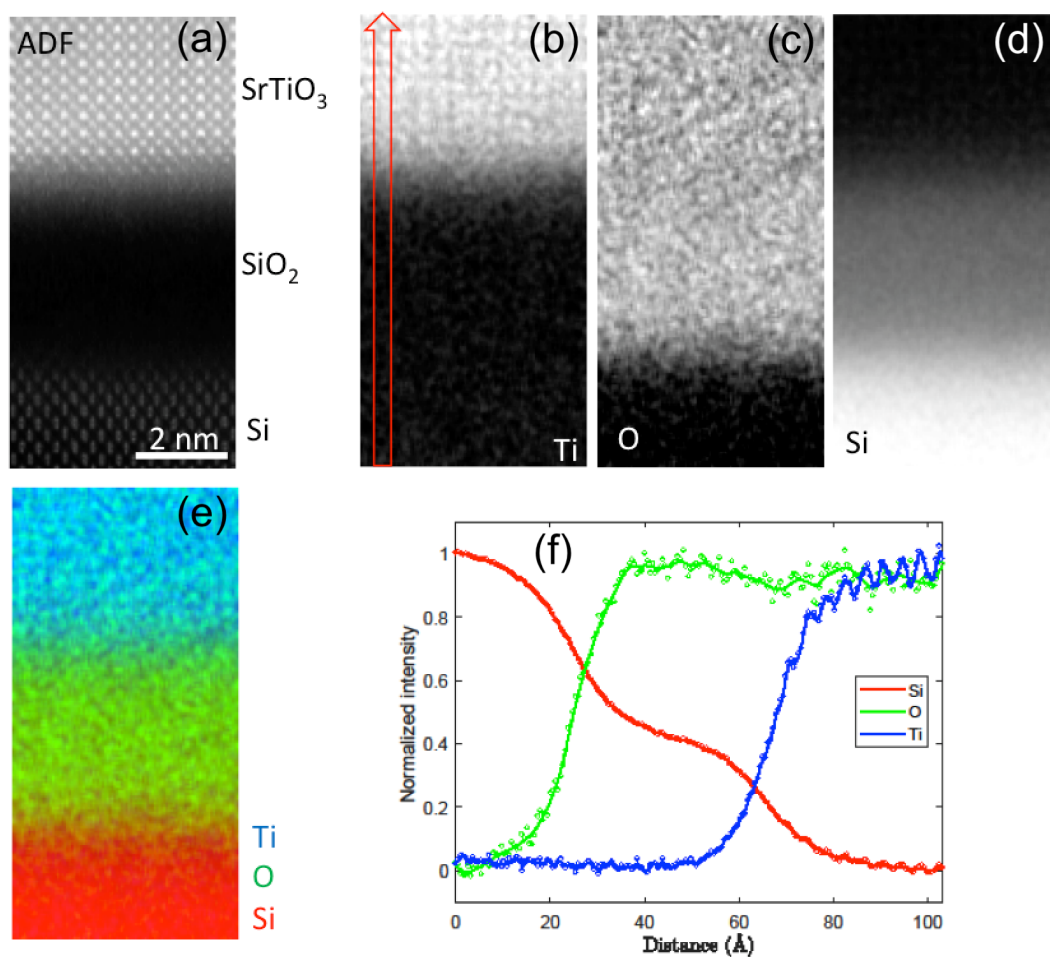


Fig. S4 (a) The HAADF-STEM image of the region in the vicinity of the SrTiO₃/Si interface of the same sample characterized in Fig. 1. STEM-EELS elemental maps of the same interfacial region for (b) Ti-*L*_{2,3}, (c) O-*K*, and (d) Si-*L*_{2,3} edges of the same interfacial region. (e) A color-coded elemental map showing that there is no perceptible interdiffusion of titanium into the SiO₂ layer. (f) Line profiles of the elemental intensity of the same region. The zero point of the line profile in (f) corresponds to the bottom side of the arrow shown in (b).

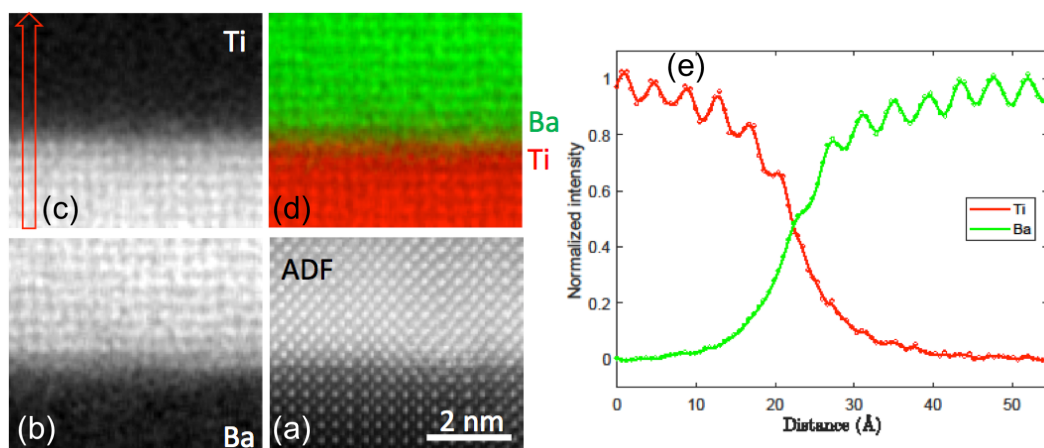


Fig. S5 (a) The HAADF-STEM image in the vicinity of the BaSnO₃/SrTiO₃ interface of the same sample characterized in Fig. 1. STEM-EELS elemental maps of (b) Ba-*M*_{4,5} and (c) Ti-*L*_{2,3} edges of the same BaSnO₃/SrTiO₃ interfacial region. (d) A color-coded elemental mapping showing that there is little perceptible interdiffusion of barium into the SrTiO₃ film. (e) Line profiles of the elemental intensity of the same region. The zero point of the line profile in (e) corresponds to the bottom side of the arrow shown in (c).